UNIVERSITÀ DEGLI STUDI DI PADOVA

Dipartimento di Fisica e Astronomia *"Galileo Galilei"*

Laurea Triennale in Astronomia

Formation Pathways of Binary Neutron Stars

Laureando:
Merli Lorenzo

Relatore:
Prof. Michela Mapelli

Correlatore:
Dott. Nicola Giacobbo

Anno Accademico 2018/2019

Abstract

With GW150914, the first detection of gravitational waves by LIGO interferometers in 2015, we had the direct proof that binary compact objects exist and merge within an Hubble time. Since then, many efforts have been made to study the formation pathways of binary compact objects. In this thesis I present the main steps that preceded this discovery, then I highlight the most important results obtained in this field. At first I review the effects of gravitational waves on binary systems, first predicted (Peters, 1964[5]) and later proved indirectly (Hulse & Taylor, 1975[6]); afterwards I discuss the main processes that drive the last phases of stellar evolution and how they affect the final fate of a binary system. In particular, I focus on natal kicks, discussing the most important studies and models about its statistical distribution and the way natal kicks affect the physical parameters of a binary. In this framework, I have analysed a population-synthesis simulation of 5 isolated binary systems. Each system was simulated twice, by changing the natal kicks. In this way there are two possible scenarios for each system. In one case the system reaches the merger, in the other the system splits. Systems with similar starting characteristics resulted to evolve in completely different ways after receiving different kicks. I discuss the main differences between the systems in the evolution of physical parameters (stellar masses, orbital separation and orbital eccentricity over time) and the way they play a key role in the fate of the systems, particularly the coalescence time.

Contents

Introduction

On September 14, 2015, the LIGO interferometers captured the event GW150914, later confirmed to be a gravitational wave (GW) signal from two merging black holes[1]. This observation paved the ground for a whole new branch of astrophysics, the GW astrophysics.
Nonetheless, the first observational evidence GWs from compact object binaries comes from Hulse & Taylor (1975)[2] and their studies on a pulsar-neutron star (NS) binary, while the prediction comes even earlier, with general relativity by Albert Einstein, 1916[3].
The latest observations via GW interferometers give crucial information on binary compact objects and open new questions. Firstly, most GW detections are associated with binary black holes (BBHs) (see figure 1.4), systems whose existence was not proved before GW150914. Moreover, the mass of BHs involved in mergers exceeds every expectation, both from observational data (known BHs, mainly from X-ray binaries, have mass under $20M_{\odot}$) and from most theoretical models (only few models predicted the existence of BHs with mass $> 30M_{\odot}$).
It is clear that we do not currently have a good enough comprehension of the processes which stars are subject to in the last phases of their evolution, processes that have dramatic consequences on binaries. The challenge of this new era of astrophysical research, hence, is to understand the processes that drive the creation of a compact object binary system, define its final fate (merger or destruction of the binary) and the way gravitational waves affect the dynamics of this system.
The aim of this thesis is to focus on a particular phenomenon of stellar evolution: the natal kick(NK). Studying natal kicks in neutron stars is important to obtain a valid estimation for the merger on binary neutron stars (BNS).
My work begins summarizing the study by Hulse and Taylor [2] on BNS as well as the latest observations made by the LIGO-Virgo collaboration until Run 2. Then I move on to natal kicks, considering the stellar evolution processes involved and the statistical distribution of NK's magnitude. The second section consists of data analysis of BNS and black hole-neutron star (BH-NS) simulations. Such data have been taken from a population synthesis code, MOBSE (Giacobbo et al. 2018)[4], elaborated and commented taking into account previous results reported. The purpose is to understand the way even slightly different natal kicks can lead to totally different binary evolutions.

Chapter 1

Binary Neutron Stars and Gravitational Waves

In 1975, Hulse and Taylor [2] wrote an article that turned out to be game changing in our knowledge of binary neuron stars. Their work is a data analysis of a binary system composed of a neuron star and a millisecond pulsar. Before talking about the results, it is important to introduce some theoretical concepts and equations.

1.1 The Predictions and the First Evidence

In this thesis I used some results from general relativity without focusing on demonstrations. We know from general relativity (GR) that the emission of gravitational waves implies a loss of orbital energy

$$E_{orb} = -\frac{Gm_1m_2}{2a} \tag{1.1}$$

Where m_1 and m_2 are the masses of the two objects that compose the binary and a is the semi-major axis. The loss of energy causes the shrinking of the orbit until the binary merges. While shrinking, the orbital frequency (ω_{orb}) becomes higher

$$2\omega_{orb} = \omega_{GW} = 2\sqrt{\frac{G(m_1+m_2)}{a^3}} \tag{1.2}$$

and the amplitude of the gravitational waves increases ($h \propto \frac{1}{a}$).
Combining the equation for the power radiated by GWs

$$P_{GW} = \frac{35}{5}\frac{G^4}{c^5}\frac{1}{a^5}m_1^2m_2^2(m_1+m_2) \tag{1.3}$$

with the derivative of orbital energy over time $\left(\frac{dE_{orb}}{dt}\right)$ in Newtonian limit

$$\frac{dE_{orb}}{dt} = P_{GW} = \frac{Gm_1m_2}{2a^2}\frac{da}{dt} \tag{1.4}$$

we can obtain the merger time scale

$$t_{GW} = \frac{5}{256}\frac{c^5}{G^3}\frac{a^4}{m_1 m_2 (m_1 + m_2)} \tag{1.5}$$

When eccentricity is included, the eq. (1.5) becomes

$$t_{GW} = \frac{5}{256}\frac{c^5}{G^3}\frac{a^4(1-e^2)^{7/2}}{m_1 m_2 (m_1 + m_2)}. \tag{1.6}$$

the equation (1.5, 1.6) is the equation derived by Peter (1964)[5] for the merger time scale for a binary system. This equation highlights some important informations. The merger timescale depends on semi-major axis, eccentricity and object masses. In addition, from eq (1.3) and (1.4) we can also derive orbital period ($\mathcal{P}$) variation over time

$$\frac{d\mathcal{P}}{dt} = -\Big(\frac{2\pi G(m_1 + m_2)}{\mathcal{P}}\Big)^{-5/3}\frac{1}{c^5}\frac{96}{5}4^{1/3} \tag{1.7}$$

Results from Hulse and Taylor

The first observational evidence that matches the GR predictions comes from the study by Hulse and Taylor (1975)[2]. The presence of a pulsar in a binary provides a nearly ideal general relativity laboratory. Indeed, we do have an accurate "clock" (the pulsar) moving at high speed in a strong gravitational field. This peculiar condition allowed Hulse and Taylor to identify the first binary neutron star due to period variation in PSR 1913+16 (as shown in figure 1.1, left panel). Then, after decades of measurements, they managed to prove the perfect match of the observations with the theoretical predictions (see figure 1.1, right panel). This was the first indirect proof of gravitational waves existence. Hulse and Taylor in 1993 received the Nobel prize for their discovery.

1.2 LIGO-Virgo

Research in gravitational waves changed completely with the construction of LIGO and Virgo interferometers. These revolutionary observatories form a net of 3 interferometers (two LIGO in the USA and one Virgo in Italy) capable of detecting space perturbations brought by GWs passing trough earth.
Both LIGO and Virgo are Michelson interferometers. In the following, I want to schematise their basic working principle. The interferometers are composed of two arms (4 km long for LIGO, 3 km for Virgo) perpendicular to each other. The laser beam, coming from a laser source, is split in the two arms by a beam splitter. At the end of each arm, there is a mirror that reflects the beam. The two beams are finally recombined by the splitter and directed into a photodetector producing an interference pattern. An incoming gravitational wave changes the optical path of the laser beams in the arms, which then changes the interference pattern recorded by the photodetector. The actual engineering on LIGO and Virgo is extremely more complicated to minimize noise (e.g.

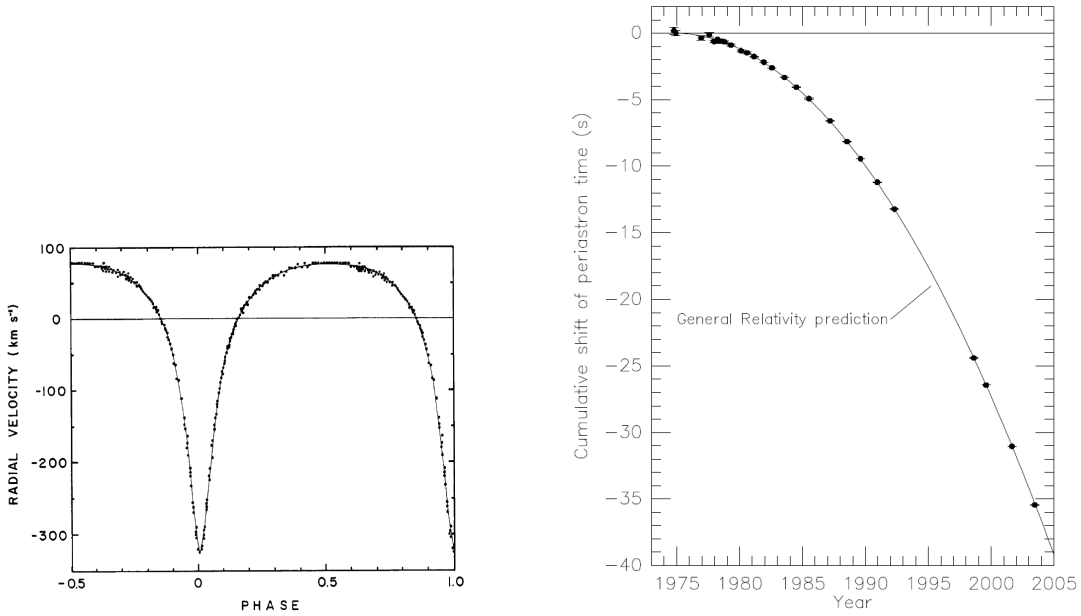

Figure 1.1: (left panel)Velocity cure of PSR 1913+16 observed by Hulse and Taylor from pulsations variation over time.[2] (right panel)Orbital decay of PSR B1913+16. The data points indicate the observed change in the epoch of periastron with date while the parabola illustrates the theoretically expected change in epoch according to general relativity[6].

seismic stabilization, beam power amplification, bring the vacuum in arms to avoid particle scattering). Several updates had been done since their first light (2007 for LIGO) that highly improved sensitivity. At the current state, the frequency range of sensitivity goes from $\sim$ 10 to 10000 Hz. More updates have already been planned to improve sensitivity even further in future runs. Figure 1,2 shows the current sensitivity curve of the three detectors of LVC.

This frequency range allows the LIGO-Virgo collaboration (LVC) to detect gravitational events only when a compact binary merges. The event duration can be of the order of tenth of seconds (for more massive BBHs) to hundreds of seconds (for binary neuron stars) but carries a great amount of information (e.g. the masses of the two objects involved, their spins, the polarization of the GW, the inclination of the system, the signal redshift, the sky location from the time delay between detections, the reference time). The figure 1.3 shows the shape of the signal in event GW150914 from both the detectors of LIGO.
In my thesis I will mainly use the information about the masses of the objects. This value can be derived analysing the shape of the detection, in particular the change of

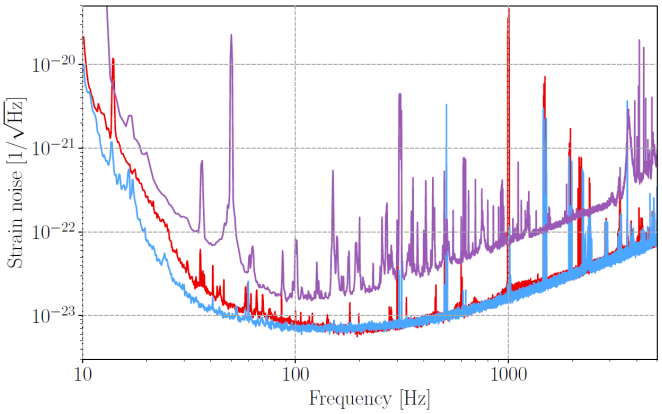

Figure 1.2: Amplitude spectral density of the total strain noise of the Virgo (violet),LIGO-Henford(LHO) (red) and LIGO-Livingston(LLO) (blue) detectors.[1]

frequency during inspiral scales with chirp mass as

$$\dot{\omega}_{GW} \propto \omega_{GW}^{11/3} m_{chirp}^{5/3}\,, \qquad m_{chirp} = \frac{(m_1 m_2)^{3/5}}{(m_1+m_2)^{1/5}} \tag{1.8}$$

and the frequency at merger scales with the total mass.

$$\omega_{GW,merger} \propto (m_1+m_2)^{-1}. \tag{1.9}$$

These two measures provide m_1 and m_2. Observational Run 3 (O3) is currently going on.

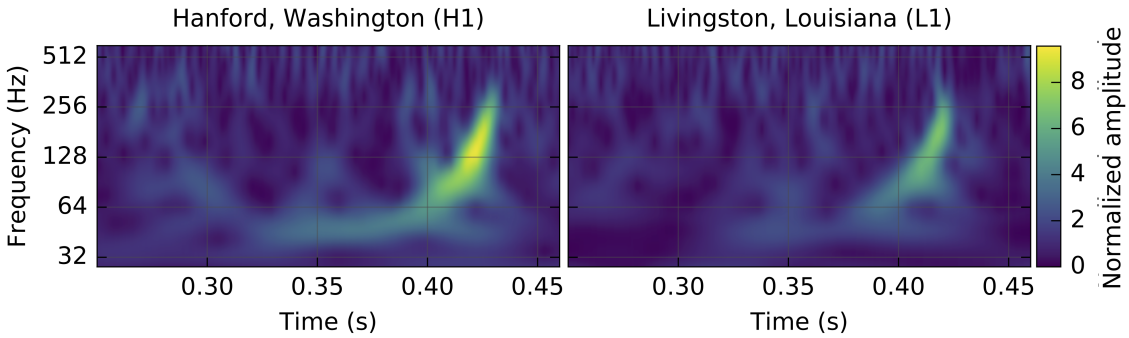

Figure 1.3: The gravitational-wave event GW150914 observed by the LIGO Hanford (left) and Livingston (right) detectors. [7]

The two past observational runs (O1 and O2) detected 11 confident GW events and a larger number of signals under the marginal triggers threshold (false alarm or high noise

signals). In the following, I report a table of the confident signals detected in run O1 and O2.

Event	$m_1/M_\odot$	$m_2/M_\odot$	$\mathcal{M}/M_\odot$	d_L/Mpc	z
GW150914	$35.6^{+4.8}_{-3.0}$	$30.6^{+3.0}_{-4.4}$	$28.6^{+1.6}_{-1.5}$	430^{+150}_{-170}	$0.09^{+0.03}_{-0.03}$
GW151012	$23.3^{+14.0}_{-5.5}$	$13.6^{+4.1}_{-4.8}$	$15.2^{+2.0}_{-1.1}$	1060^{+540}_{-480}	$0.21^{+0.09}_{-0.09}$
GW151226	$13.7^{+8.8}_{-3.2}$	$7.7^{+2.2}_{-2.6}$	$8.9^{+0.3}_{-0.3}$	440^{+180}_{-190}	$0.09^{+0.04}_{-0.04}$
GW170104	$31.0^{+7.2}_{-5.6}$	$20.1^{+4.9}_{-4.5}$	$21.5^{+2.1}_{-1.7}$	960^{+430}_{-410}	$0.19^{+0.07}_{-0.08}$
GW170608	$10.9^{+5.3}_{-1.7}$	$7.6^{+1.3}_{-2.1}$	$7.9^{+0.2}_{-0.2}$	320^{+120}_{-110}	$0.07^{+0.02}_{-0.02}$
GW170729	$50.6^{+16.6}_{-10.2}$	$34.3^{+9.1}_{-10.1}$	$35.7^{+6.5}_{-4.7}$	2750^{+1350}_{-1320}	$0.48^{+0.19}_{-0.20}$
GW170809	$35.2^{+8.3}_{-6.0}$	$23.8^{+5.2}_{-5.1}$	$25.0^{+2.1}_{-1.6}$	990^{+320}_{-380}	$0.20^{+0.05}_{-0.07}$
GW170814	$30.7^{+5.7}_{-3.0}$	$25.3^{+2.9}_{-4.1}$	$24.2^{+1.4}_{-1.1}$	580^{+160}_{-210}	$0.12^{+0.03}_{-0.04}$
GW170817	$1.46^{+0.12}_{-0.10}$	$1.27^{+0.09}_{-0.09}$	$1.186^{+0.001}_{-0.001}$	40^{+10}_{-10}	$0.01^{+0.00}_{-0.00}$
GW170818	$35.5^{+7.5}_{-4.7}$	$26.8^{+4.3}_{-5.2}$	$26.7^{+2.1}_{-1.7}$	1020^{+430}_{-360}	$0.20^{+0.07}_{-0.07}$
GW170823	$39.6^{+10.0}_{-6.6}$	$29.4^{+6.3}_{-7.1}$	$29.3^{+4.2}_{-3.2}$	1850^{+840}_{-840}	$0.34^{+0.13}_{-0.14}$

Figure 1.4: Table of the eleven confident gravitational waves signals revealed by the LIGO-Virgo collaboration in O1 and O2 (GW170817 is the neutron stars merger). The first two columns shows the initial mass of each compact object, $\mathcal{M}$ is the chirp mass, d_L the luminosity distance of the source and z its Redshift. [1]

Chapter 2

The Birth of a Compact Remnant

Massive stars ($M>8M_{\odot}$) are destined to undergo supernova explosion and eject their envelope, to give birth to a compact object. The mechanisms involved are extremely complex and barely understood. The mass of compact remnants, hence, is highly uncertain and the presence of a companion adds even more complexity to this problem. Below I briefly present the major steps that a star takes trough the end of its life.

2.1 Stellar Winds and Supernovae

The mass of a star can change during his life. Estimating the pre-SN mass is tremendously important for the study of compact objects.
The outflow of gas from stellar atmospheres is called stellar winds. This outflow can have different sources. In cold stars (e.g. AGB stars), the main driver of stellar winds is radiation pressure on cold dusty layers in outer regions. In hot massive stars, the outflow is induced by the coupling between the momentum of photons and the momentum of metal ions present in the stellar photosphere. Understanding the mass loss of a star during its lifetime is not a trivial issue. Advanced work made by Vink et al. (2001)[8], accounting for multiple scattering, define $\dot{m} \propto Z^{0.85} v_{\infty}^{p}$ [1] for stars with $T_{eff} \gtrsim 25000K$.
The situation is even more uncertain for post-main sequence stars such as Wolf-Rayet.
Other aspects of massive star evolution play a considerable role in defining the pre-SN mass of a star. The magnetic field can be one of these aspects. On the surface, the magnetic field can confine and strongly quench stellar winds. Another important ingredient is the rotation. On the one hand, rotation acts by increasing stellar luminosity, on the other, it induces chemical mixing. This leads to lager helium and carbon-oxygen core which have strong implications in the following phase.
As the mass of the central degenerate iron-core reaches the Chandrasekhar mass ($M_{ch} \approx 1,44 M_{\odot}$), core-collapse is triggered. The mechanisms involved are still highly uncertain. The main actors are:

[1] v_{∞}^{p} is called terminal velocity and is the maximum velocity of stellar winds, reached at theoretically infinite distance, when acceleration is equal to zero.

- the degeneracy pressure of relativistic electrons becomes insufficient to support the equilibrium;
- protons capture electrons producing neutrinos and decreasing the degeneracy pressure .

The core rapidly falls into a new state where equilibrium can be carried by degeneracy pressure of neutrons. In less than a second the core shrinks from thousands of Km to a few ten. This shock liberates an incredible amount of Gravitational energy: $W \approx 5 \times 10^{53} erg \left(\frac{m_{PNS}}{1.4 M_{\odot}}\right)^2 \times \left(\frac{10 km}{R_{PNS}}\right)$ where m_{PNS} and R_{PNS} are the mass and radius of the proto-neutron star (PNS). Astrophysicists are trying to explain the way this gravitational energy can be converted into kinetic and other forms of energy triggering the SN explosion. The convective supernova engine is the best investigated model. The main steps of this mechanism are:

- The collapsing core drives a bouncing shock.
- This shock reverses the infall of matter from the outer layers.
- The source of energy in the shock is provided by neutrinos; once the shock is diffuse enough, neutrinos leak out and the shock stalls.
- The region between the proto-neutron star surface and the stalling radius becomes connectively unstable because of cooling.
- Such convective instability can convert the energy escaping from the proto-neutron star to kinetic energy pushing the convective region outward
- If the convective region overcomes the ram pressure -P_{ram} is the pressure exerted by the outer layer that works against the inner layer motion- of the infalling material, the shock is revived and the explosion is launched. If not, the SN fails.

2.2 Compact Remnants

All the uncertainties introduced previously suggest that it is impossible to have an accurate estimation of the remnant mass. However, few robust features can be drawn. Stellar winds are the most influential effect for stars with Zero Main Sequence mass $m_{ZAMS} \geq 30 M_{\odot}$. Stellar winds depend on metallicity. For metal-poor stars ($0.1 Z_{\odot}$) mass loss is almost negligible and the total final mass, as well as the Carbon-Oxygen final mass may be sufficiently large to avoid core collapse. In this case the star may form a massive BH by direct collapse unless a pair-instability or a pulsational-pair instability SN occurs. At high metallicity ($\approx Z_{\odot}$) stellar winds lead to an efficient mass loss. It may bring to a small final mass (m_{fin}) and carbon-oxygen mass (m_{CO}). In this condition core-collapse can be triggered, resulting in a relatively small remnant. Considering stars with relatively low ZAMS mass ($7 < m_{ZAMS} < 30 M_{\odot}$), stellar winds lose importance,

regardless of the metallicity. In this scenario, the characteristics of SN explosion are crucial to define the final mass of the remnant.

2.3 Binaries: Mass Transfer and Common Envelope

If we consider binary stars, even more complications add on. Only if the system is sufficiently wide for its entire evolution, then the evolution of the two stars can be considered separately. The most important binary-evolution processes -when their orbit are narrow enough to interact with each other- are mass transfer and common envelope. Mass transfer is an exchange of matter between the two objects in the binary. The principle that drives this phenomenon can be stellar winds or Roche-lobe filling. When the stellar winds occur, the mass lost by the star can be captured by its companion. The mean mass accretion rate by stellar winds can be described, according to Hurley et al.(2002)[9], as:

$$\dot{m}_2 = \frac{1}{\sqrt{1-e^2}}\left(\frac{Gm_2}{v_w^2}\right)^2 \frac{1}{\left[1+\left(\frac{v_{orb}}{v_w}\right)^2\right]^{3/2}}\dot{m}_1. \tag{2.1}$$

Where G is the gravitational costant, m_2 represents the mass of the accreting star, v_w represents the velocity of the wind, $\alpha_w \approx 3/2$ is an efficiency constant, a represents the semi major axis of the binary, $v_{orb} = \sqrt{G(m_1+m_2)/a}$ represents the orbital velocity of the binary and $\dot{m}$ represents the mass loss Roche lobe overflow is commonly more efficient than stellar winds. The Roche lobe of a star in a binary system is the maximum equipotential surface around the star within which matter is bounded to the star. See figure 2.1 for a representation of the Roche lobe. The approximated shape of the Roche lobe is given by[10]:

$$r_{L,1} = a\frac{0.49q^{2/3}}{0.6q^{2/3}+\ln(1+q^{1/3})} \tag{2.2}$$

where a is the semi-major axis of the binary and $q = m_1/m_2$ (m_1 and m_2 are the masses of the two stars in the binary). The Roche lobe of the other star ($r_{L,2}$) can be obtained by swapping the indexes. The Roche lobes of the two stars in a binary are thus connected by the L1 Lagrangian point. Since the Roche lobes are equipotential surfaces, matter orbiting at or beyond the Roche lobe can flow freely from one star to the other. We say that a star overfills its Roche lobe when its radius is larger than the Roche lobe. If a star overfills its Roche lobe, a part of its mass flows toward the companion star which can accrete (a part of) it. The former and the latter are thus called donor and accretor star, respectively.
If mass transfer is dynamically unstable (the star expands faster than the Roche lobe) or both stars overfill their Roche lobe, then the binary is expected to merge, or to enter common envelope (CE). If two stars enter in CE, their envelopes stop co-rotating with their cores. The two stellar cores are embedded in the same non-corotating envelope and start spiraling in as an effect of gas drag exerted by the envelope, losing orbital energy in the meanwhile. Part of this energy goes into heating of the envelope, making it more loosely bound. This process can lead to different results:

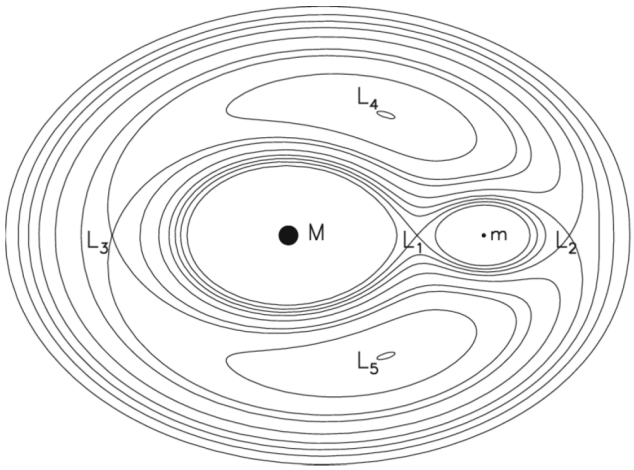

Figure 2.1: Equipotential surfaces and Lagrangian points of a binary system.

- The heating can lead to the ejection of the envelope. The system survived as a binary of naked stellar cores (or a compact remnant and a naked stellar cores). The orbital separation of this two object is considerably smaller than the initial orbital separation of the binary.
- If the envelope is not ejected, the two cores (or the compact remnant and the core) spiral in until they eventually merge. This premature merger of a binary during a CE phase prevents the binary from evolving into a binary compact object.

Chapter 3

Natal Kicks

The most simple stellar evolution models use the approximation of spherical symmetry for supernovae. However, supernovae are not symmetrical either in neutrino flux or ejecta mass. The main consequence of this anisotropy is that supernovae impress a certain velocity to compact remnants. In addition, if the SN occurs in a binary star, we expect the so-called Blaauw kick to affect the orbital properties of the binary system, even if mass loss is completely symmetric. The natal kick has serious implications in binary compact objects because it can either unbind the system or change its orbital properties. For example, a SN kick can increase the orbital eccentricity or misalign the spins of the two members of the binary. The estimations of natal kicks magnitude are extremely uncertain, especially for BHs. As to neuron stars we have some more information to work on. This information comes from observational surveys and simulation models. In the following I reported some of the most significant studies on natal kicks statistical velocity distribution, in order to have a clear picture of the basic observational evidences as well as the state of art simulation models.

3.1 Statistical Distribution of v_k

Most observational estimates of natal kicks come from pulsar proper motions. Hobbs(2005)[11] analysed the proper motions of 233 Galactic pulsar. The majority of the proper motions (58 %) are derived from pulsar timing methods, 41 percent using interferometers and the remaining 1 percent using optical telescopes. Restricting their analysis to the 73 pulsars younger than $\sim 3Myr$ they fit a Maxwellian distribution for the natal kick velocity, with one-dimensional root-mean-square velocity $\sigma = 265 kms^{-1}$. Figure 3.1 report this work.

This result, however, is still under debate. Other works (e.g. Fryer et al. (1998) [12] and Verbunt et al. (2017) [13]) suggest a double Maxwellian, with the first peak at low velocities and a second peak at high velocities. Figure 3.2 shows the comparison between those models and the single Maxwellian model.

Moreover, Beniamini et al. (2016)[14] find a strong preference for small natal kicks in binary neutron stars. As to BHs, there are evidence of small natal kicks from X-ray binaries but also a requirement of high natal kicks to explain the position of BH with

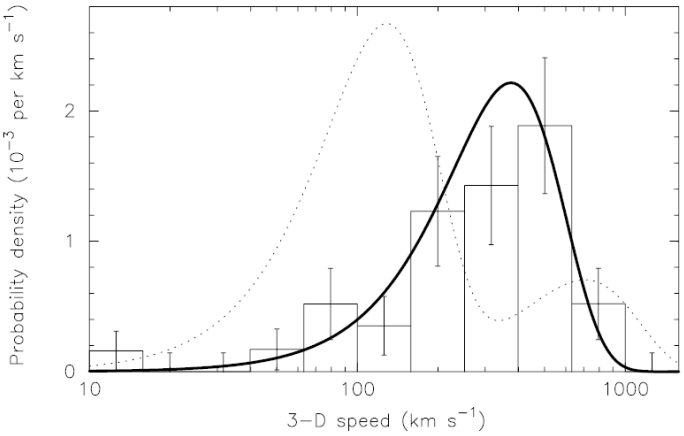

Figure 3.1: The 3D velocity distributions Hobbs obtained from the observed 2D distributions. The solid curve is the best-fitting Maxwellian distribution to the histogram with $\sigma = 265 kms^{-1}$.[11]

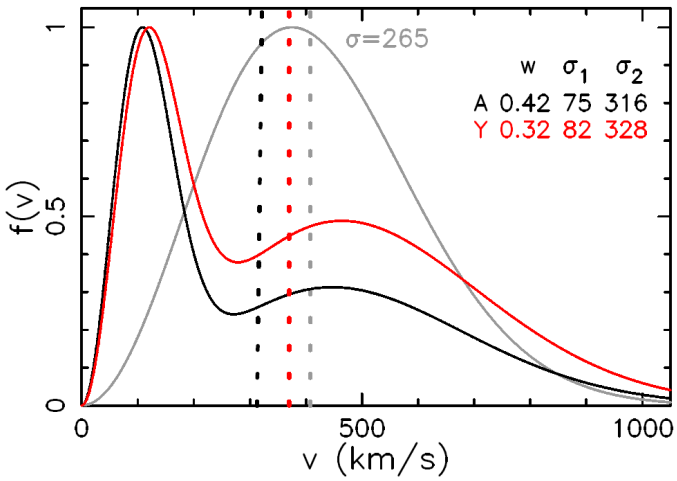

Figure 3.2: The comparison between single Maxwellian distribution with $\sigma = 265 kms^{-1}$ and the double Maxwellian that best fit the youngest pulsars. (The vertical dotted lines indicates the median velocities)[13]

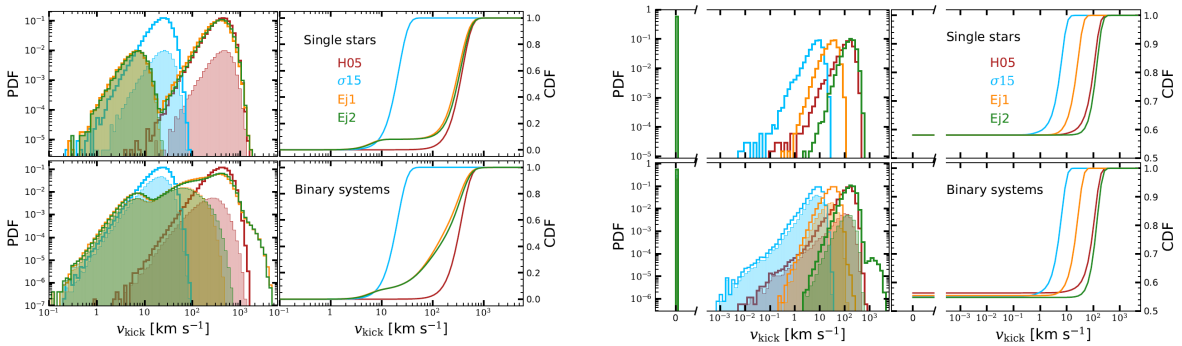

Figure 3.3: (Left panels): Probability distribution function (PDF) of natal kicks for all NSs formed both in single stars (top) and from binary systems (bottom) using different models (in orange the prediction of the model treated here ($v_{kick} \propto f_{H05} m_{ej} m_{REM}^{-1}$)). Right-hand panels: cumulative distribution function (CDF) of natal kicks for all NSs. (Right panels) same but for BHs. [4]

respect to the Galactic plane (Repetto et al. (2012)[15]).
Recently a more comprehensive prescription has been proposed (Giacobbo & Mapelli (2019)) [4] which can be written in the form

$$v_{kick} \propto f_{H05} m_{ej} m_{REM}^{-1} \tag{3.1}$$

where f_{H05} express the singular Maxwellian distribution with $\sigma = 265 kms^{-10}$, m_{ej} is the mass of the ejecta, m_{REM} is the mass of the remnant and v_{kick} express the kicks' magnitude distribution. So they took the singular Maxwellian distribution with $\sigma = 265 kms^{-10}$ from Hobbs[11] and they also take into account the role that the mass of the ejecta and the mass of the remnant play in kicks' magnitude distribution. Figure 3.3 shows the comparison between models made by Giacobbo & Mapelli.

For the single star evolution, the distribution of v_{kick} has a good match with the high-velocity peak observed by Hobbs [11] as well as low peak[12][13]. In addition, the dependence on m_{ej} and m_{REM} highlights the physical meaning of those peaks (one coming from core-collapse supernovae and the other one from electron capture supernovae and direct collapses). On the other hand, this model predicts a totally different distribution of natal kicks in binary systems. According to this model, binary evolution tends to increase the number of neuron stars with small kicks. The reason behind this trend is that mass transfer (explained in sec. 2.1.1) reduces m_{ej}. Nevertheless, this model predicts that binary evolution also triggers the formation of few neutron stars with even larger kicks than in the case of single-star evolution. The merger rate obtained using these assumptions meets the expectation from state of art studies[1].

3.2 Dynamics of Natal Kicks

Here I will introduce the formalism used by Hurley(2002)[9] to describe the impact of natal kicks on angular momentum (and thus, on orbit characteristics).
Consider a frame of reference in which the pre-supernova centre-of-mass is at rest, the primary star is about to explode and the secondary is at the origin. The initial orbit is in the XY-plane so that the initial specific angular momentum vector is directed along the positive Z-axis, and the separation vector $\mathbf{r} = \mathbf{r_1} - \mathbf{r_2}$ is directed along the positive Y-axis, as shown in Figure 3.4. The relative velocity of the star is

$$\mathbf{v} = -v_{orb}(sin\beta\mathbf{i} + cos\beta\mathbf{j}) \tag{3.2}$$

where β is the angle between $\mathbf{r}$ and $\mathbf{v}$ and is such that:

$$\sin\beta \;=\; \left[\frac{a^2(1-e^2)}{r(2a-r)}\right]^{1/2} \tag{3.3}$$

$$\cos\beta \;=\; \frac{e\sin E}{(1-e^2\cos^2 E)^{1/2}} \tag{3.4}$$

and E is the eccentric anomaly in Kepler's equation

$$\mathcal{M} = E - e\sin E \tag{3.5}$$

for mean anomaly $\mathcal{M}$ which varies uniformly with time between 0 and 2π. The orbital speed is defined by

$$v_{orb}^2 = \dot{r}^2 + r^2\dot{\theta}^2 = GM_b(\frac{2}{r} - \frac{1}{a})\ ,\ M_b = M_1 + M_2 \tag{3.6}$$

As well as losing an amount of mass ΔM_1 the primary star is subject to a kick velocity $\mathbf{v}_k$ during the supernova explosion so that:

$$M_1 \;\rightarrow\; M_1' = M_1 - \Delta M_1$$

$$M_b \;\rightarrow\; M_b' = M_b - \Delta M_b$$

$$\mathbf{v}_1 \;\rightarrow\; \mathbf{v}_1' = \mathbf{v}_1 + \mathbf{v}_k$$

where

$$\mathbf{v}_k = v_k(\cos\omega\cos\phi\mathbf{i} + \sin\omega\cos\phi\mathbf{j} + \sin\phi\mathbf{k})\ ,\ v_k = \mid \mathbf{v} \mid \tag{3.7}$$

Here $\mathbf{i}$, $\mathbf{j}$ and $\mathbf{k}$ are unit vectors in the X, Y and Z directions respectively. We assume the separation is constant as the explosion is instantaneous. To find the separation at the moment of explosion we randomly choose a mean anomaly ⇳ and then solve eq.(3.4) for the eccentric anomaly E using a Newton-Raphson method. Then

$$r = a(1 - e\cos E)\ ,\ r = |\mathbf{r}| \tag{3.8}$$

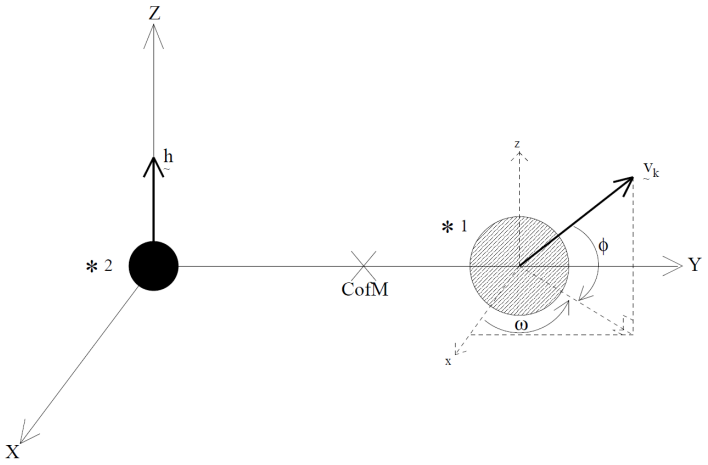

Figure 3.4: The binary and supernova kick geometry.[9]

in terms of the initial semi-major axis and eccentricity. This is necessary because the binary is evolved using values averaged over an orbital period so that the exact separation at any one time is not known for an eccentric orbit. After the supernova, the new relative velocity is

$$\mathbf{v}_n = \mathbf{v} + \mathbf{v}_k = (v_k \cos\omega \cos\phi - v_{orb} \sin\beta)\mathbf{i} + (v_k \sin\omega \cos\phi - v_{orb} \cos\beta)\mathbf{j} + v_k \sin\phi\mathbf{k}$$

From eq. (3.5) it must be true that

$$v_n^2 = GM_b'\Big(\frac{2}{r} - \frac{1}{a_n}\Big) \tag{3.9}$$

for the new orbital parameters, where

$$v_n^2 = |\mathbf{v}_n|^2 = v_k^2 + v_{orb}^2 - 2v_k v_{orb}(\cos\omega \cos\phi \sin\beta + \sin\omega \cos\phi \cos\beta). \tag{3.10}$$

This can be solved for the semi-major axis a_n of the new orbit. The specific angular momentum of the new system is

$$\mathbf{h}' = \mathbf{r} \times \mathbf{r}_n \tag{3.11}$$

so it follows from

$$l = a(1 - e^2) = \frac{h^2}{GM_b} \tag{3.12}$$

(where l is the semi-latus rectum) that

$$GM_b a_n(1 - e^2) = |\mathbf{r} \times \mathbf{v}_n|^2 \tag{3.13}$$

where

$$|\mathbf{r} \times \mathbf{v}_n|^2 = r^2[v_k^2 \sin^2\phi + (v_k \cos\omega \cos\phi - v_{orb} \sin\beta)^2] \tag{3.14}$$

With this we can solve for the new eccentricity e_n of the orbit. If either $a_n \leq 0$ or $e_n > 1$ then the binary does not survive the kick. The angle ν between the new and old angular momentum vectors is given by

$$\cos\nu = \frac{v_{orb}\sin\beta - v_k\cos\omega\cos\phi}{[v_k^2\sin^2\phi + (v_k\cos\omega\cos\phi - v_{orb}\sin\beta)^2]^{1/2}}. \tag{3.15}$$

An amount of mass ΔM_1 is ejected from the primary, and hence from the system, so that the new centre-of-mass has a velocity

$$\mathbf{v}_s = \frac{M_1'}{M_b'}\mathbf{v}_k - \frac{\Delta M_1 M_2}{M_b' M_b}\mathbf{v} \tag{3.16}$$

relative to the old centre-of-mass frame. To determine the kick velocity it is necessary to choose vk, the magnitude of $\mathbf{v}_k$, ϕ, the angle between $\mathbf{v}_k$ and the orbital plane, and ω, the angle between the projection of $\mathbf{v}_k$ on to the orbital plane and the X-axis, from appropriate distribution functions. The kick direction (ϕ) is uniform over all solid angles and ω is uniformly distributed between 0 and 2π. However, in my data analysis, I only take into account kick magnitude v_k. The distribution chosen in the MOBSE code follows the model suggested by Giacobbo & Mapelli[4], as explained in the next chapter.

Chapter 4

Data Analysis

In this chapter, I will analyse and discuss data regarding 5 simulated isolated binaries of neutron stars. These data come from a population synthesis code (MOBSE)[4]. The binaries start with different characteristics and follow a different evolution paths. Originally, all 5 system resulted to merge, but they all were simulated a second time, with different kicks, to highlight that even binaries that start with the same characteristics can reach a different end (he second choice of the kick disrupts the systems). The aim is to understand the way the system reacts to the kicks. First, I want to introduce briefly the way the data are generated, then I will show and discuss the plots I made from the data.

4.1 MOBSE

MOBSE (Massive Object in Binary Stellar Evolution) is a population-synthesis code developed by Giacobbo and al. (2018)[16]. This code is a customized version of BSE (Binary Stellar Evolution), Hurley et al. (2000, 2002)[17] [9] which takes into account the state of art studies on star evolution. Here I summarize the main assumptions that MOBSE features.

- For the stellar evolution it uses the polynomial fitting formulas developed by Hurley et al. (2000) [17].
- For stellar winds and mass loss it uses the formalism described in Giacobbo & Mapelli (2018)[18].
- For the natal kicks it uses the natal kicks distribution described in Giacobbo & Mapelli (2019)[4].
- For the binary evolution it uses mass transfer, common envelope, tidal evolution and gravitational wave decay as described in Hurley et al. 2002 [9].
- Fore the supernovae it uses the formalism developed by Fryer and al. (2012)[19]

4.2 Results

To visualize the way the systems evolve, for each binary I plotted its main characteristics (masses, orbital eccentricity and semi-major axis) over time from the two simulations.

4.3 Discussion

Merger scenario

Systems 1 and 2 (figure 4.1) follow a very similar path for most of their lives. They are both composed of a massive primary (above 70 $M_\odot$) and a smaller companion ($\approx 15 M_\odot$). The primary evolves faster and the mass loss, due to stellar winds, is efficient (in all the other stars considered, mass loss due to stellar winds is negligible). At $\approx$ 4 Myr a Roche lobe filling and, later, a common envelope set in. In this phase the orbital separation decreases and the eccentricity goes to 0. When the process ends, the primary has become a naked helium core that will soon become a BH, while the companion is still in main sequence. The evolution goes on until a second common envelope ($\approx$ 13 Myr) in secondary's red giant branch. Here the system shrinks again. The result is a binary composed of a BH and a naked core that will become a neutron star. From this point on masses and eccentricities will no more be affected, while separation decreases gradually due to GWs until the system merges. Despite all those similarities, the two systems don't share the same fates. The kick of the primary (at t$\approx$4.3 Myr for both systems) has a small effect on the dynamics in either binary (according to v_k distribution used). The natal kick of the companion ($t \approx 15 Myr$ for both systems), however, is different. In system 1 (Figure 4.1, left panels) the eccentricity undergoes a negligible change while in system 2 (Figure 4.1, right panels) the eccentricity becomes close to 1. As we see in sec. 1.1, the merger time strongly depends on eccentricity; this is the reason why the system 1 reaches the coalescence in 4 Gyr and the system 2 merges in 190 Myr.
Systems 3 and 4 (Figure 4.2) have lower masses than systems 1 and 2, and have higher separation. The two stars in these binaries do not affect each other in the early phases of their lifetimes. In both systems common envelope occurs after the stars enter the red giant branch ($t \approx 20 Myr$ for system 3, $t \approx 15 Myr$ for system 4). At the end of the common envelope phase, the systems have lost most of their mass, the remnants are two naked helium cores that will become neutron stars and finally merge. Here again, the natal kicks that occur in the moment of the neutron star formation make the differences in the system's epilogue. In system 3, the kick received by the primary ($t \approx 20 Myr$, right after common envelope phase), increases the eccentricity from 0 to 0.72. However, when the companion reaches the supernova phase ($t \approx 23 Myr$), it receives a kick that decreases eccentricity and separation. The result is that the system merges in $\approx$8 Gyr. (according to eq.1.6, low eccentricity and low mass contribute to increasing t_{GW}). The system 4 starts with high eccentricity, but after CE the orbit is almost circular (e=0) both the kicks of the two stars, one at $t \approx 16 Myr$ and the other at $t \approx 17 Myr$ decrease separation and increase eccentricity, leading the system to reach coalescence in a very short time ($\approx 20 Myr$). The system 5 (Figure 4.3) follows a different path. The starting

masses are lower than the other systems (10 $M_\odot$ and 7.5 $M_\odot$) and the orbital separation is very low ($\approx 80R_\odot$). The Roche lobe infilling sets in right after the primary enter the Hertzsprung gap ($t \approx 24Myr$). In this phase, the system undergoes a mass transfer process that almost doubles the mass of the companion (from 7.5 $M_\odot$ to 15 $M_\odot$) leaving just the He core to the primary. The first kick (that occurs at $t \approx 29Myr$) increases separation and eccentricity. This new equilibrium survives until the companion enters the asymptotic giant branch ($t \approx 33Myr$). Here its radius increases, and a common envelope process begins and brings once again the eccentricity close to 0. At the end of CE all the envelope is ejected. The neutron star and the newly formed He core are very close. The second kick ($t \approx 35Myr$) occurs without changing the mass of the primary. The result of this kick is a highly eccentric and close BNS that will merge 70 Myr after its formation ($t \approx 108Myr$).

Disrupt Scenario

In this scenario, the evolution of the system naturally follows the same steps as the previous until the first kick takes place. The masses and times at which kicks occur, do not undergo relevant changes, while eccentricity and separation can be modified completely. When the binary is disrupted. Here I discuss the difference the kinks make in each system.
In system 1 (See figure 4.1, left, dashed line), the kick received by the black holes in the moment of its formation has almost no impact on physical parameter. The system remains a close binary until the companion receives a kick (while becoming a neutron star) that unbinds the binary ($t \approx 15Myr$).
In system 2 (See figure 4.1, right, dashed line), the kick received by the black hole (probably a Blaauw kick, as the first) strongly increases separation and eccentricity of the binary, then disrupted by the kick of the companion ($t \approx 14Myr$).
In system 3 (See figure 4.2, left, dashed line), the kick that the primary receives is the one that splits the binary ($t \approx 20Myr$). From there, the evolution continues separately and the companion receives a kick as soon as the binary does not exist any more.
In system 4 (See figure 4.2, right, dashed line), the primary becomes a neutron star while the system is still in common envelope phase, decreasing its separation and increasing its eccentricity. The second kick stresses even more the system and in a short time, the binary breaks apart ($t \approx 17Myr$).
System 5 (See figure 4.3, dashed line) does not actually disrupt: the primary becomes a neutron star while the system is still in common envelope phase like system 4. The effect of this kick, however, is to increase separation without having a big impact on eccentricity (that slightly increases). The system at $t \approx 33Myr$ enters common envelope phase and it collide right after. The companion does not undergo supernova phases and only the neuron star (whose mass remains virtually unchanged) survives.

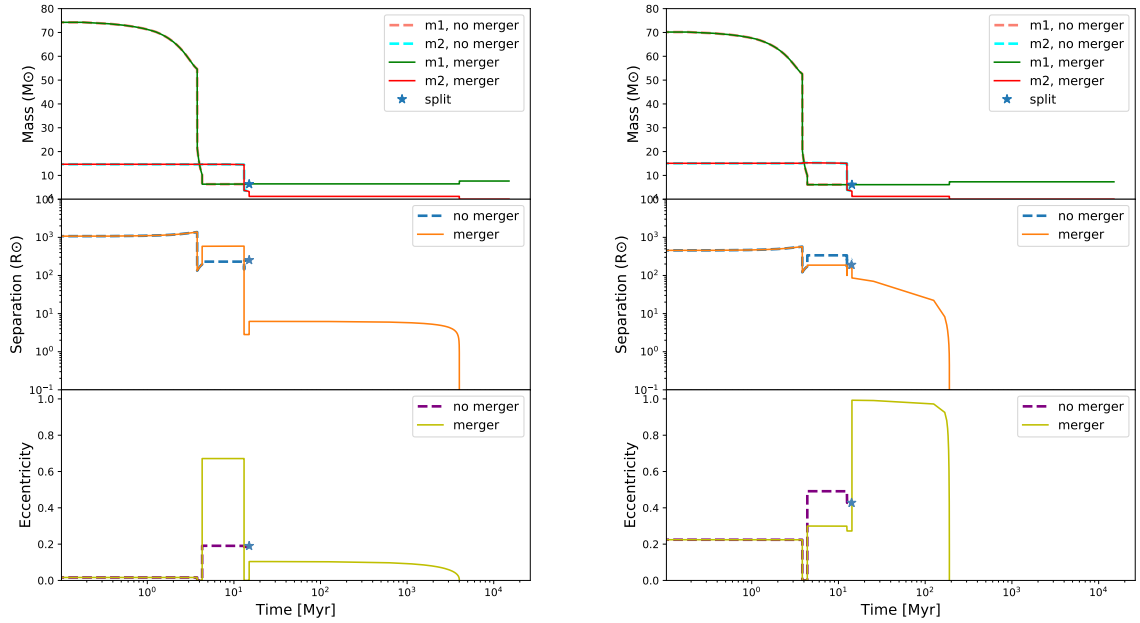

Figure 4.1: Data plot of systems 1 and 2 (respectively left and right panels). Top panels: evolution of the mass of the primary and the companion as a function of time. Middle panel: evolution of the orbital separation as a function of time. Bottom panels: evolution of the eccentricity as a function of time. In all panels, the solid line shows the simulation in which the binary merges by GW emission, while the dashed line indicates the simulation in which the binary disrupts.

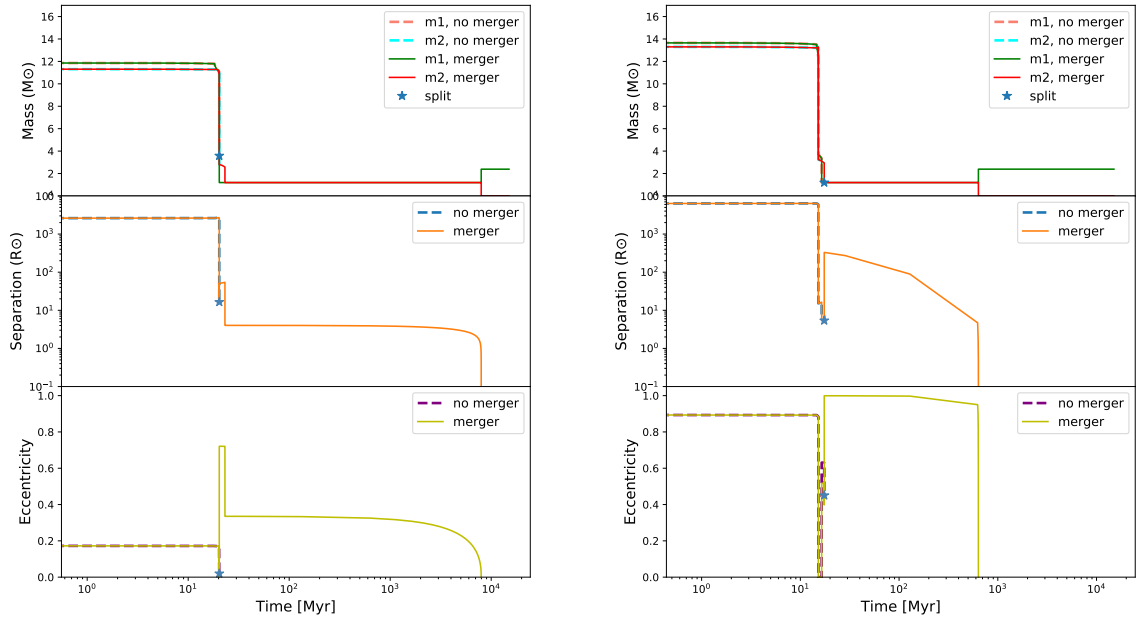

Figure 4.2: Data plot of system 3 and 4 (respectively left and right panels), same formalism as figure 4.1

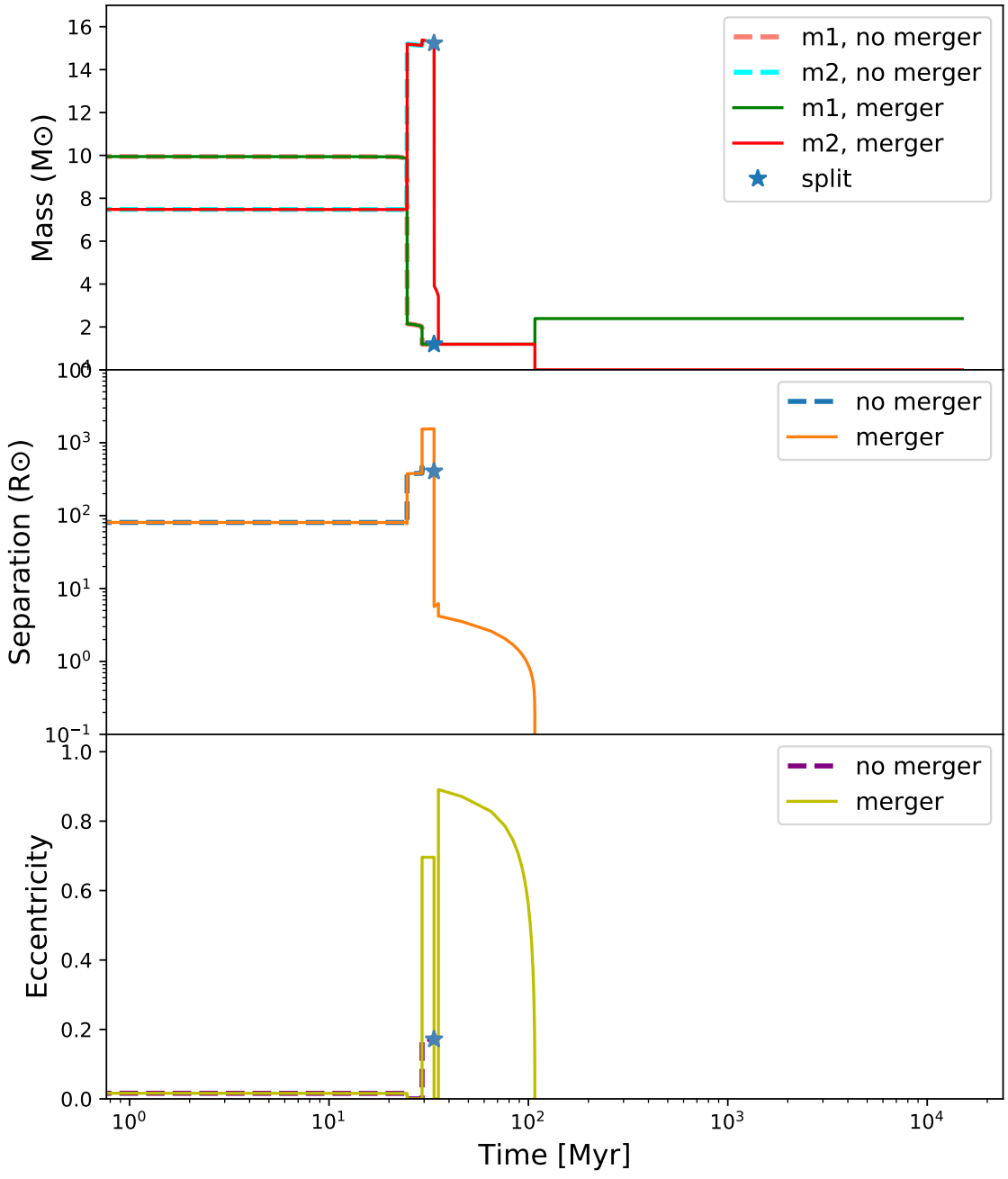

Figure 4.3: Data plot of system 5, same formalism as figure 4.1

Conclusions

In the first part of this thesis, I reviewed the main steps made in gravitational waves astrophysics. Starting from the theoretical predictions of Peters[5] then the first indirect evidence by Hulse & Taylor[2] to reach state of art observation with LIGO-Virgo collaboration. Afterwards I highlighted the main processes that drive the last phases of stellar evolution and how they affect the final fate of a binary system. In the third part I introduced the phenomenon of natal kick, the most important studies on this framework and the main issues of this phenomenon. In the last part, I analysed a set of binary stars simulated by means of a population-synthesis code. For each set of starting physical parameters (stellar masses, orbital separation and orbital eccentricity) I studied two evolution pathways, one that ends with the coalescence of the two objects, the other that ends with the split of the binary. In every simulation, the natal kicks of the two stars becoming compact objects turned out to play a key role in the definitions of the evolutionary pathways followed by the system. In particular, the equation 1.4 expresses fact that binaries reach coalescence by losing energy through gravitational waves emission. Equation 1.6 highlights the dependence of merger time from masses of the object, orbital separation and eccentricity. In sec. 3.2 it is reported a formalism that explains the way natal kicks affect these quantities. Another elements that has to be considered in order to analyse the results is that the velocity distribution used in the population-synthesis code depends on masses of ejecta and remnants (as explained in sec 3.1). For examples a naked core that has lost its envelope after CE phase (system 3, figure 4.2, left) is more likely to receive a lower kick than a star who has accreted mass in a mass transfer phenomenon and reaches supernova phase with a large envelope (system 5, figure 4.3). We can see that all these phenomena affect the system evolution. The merger time decreases enormously when the kick increases the orbital eccentricity. Roche lobe filling and common envelope phase completely change separation and masses. The kick, however, can end this phase (system 3-5, figure 4.2, 4.3) leading the ejection of the envelope or triggering the collision of the cores so that the system becomes a single star. If the system manages to survive after the two kicks, it slowly shrinks due to GW emission until it reaches coalescence within an Hubble time. In all the simulations that lead to the disruption of the system the splits occur soon after the first (system 3, fig 4.2, left) or the second (system 1,2,4,5, figures 4.1, 4,2 (right) 4.3) kick. System 5 presents a peculiar situation. In the early stages, its life undergoes mass transfer phenomenon via Roche lobe infilling. When it ends, the mass of the primary has become 1.2 $M_{\odot}$ (from

$\approx 10M_{\odot}$) and the mass of the companion has become 15.2 $M_{\odot}$ (from $\approx 7M_{\odot}$). In the merger simulation, after the kick of the primary the separation and the eccentricity are high. After 4 Myr the two stars comes into contact. When this phenomenon happens the companion loses all its envelope. So, when it reaches the supernova phase, the system survives (low ejecta mass leads to lower kicks) with low separation and high eccentricity thus making the two objects collide in 107 My. In disrupt simulation instead, after the primary undergoes supernova phase and receive a kick, the system is close and and has low eccentricity. The companion, in this case, does not lose its envelope until a common envelope sets in. Here the code reports that the primary star does not exist any more. Probably the core of the companion and the neutron star collided. The code in this case sees the mass of the companion as mass accreted by the NS. This mass is soon ejected leaving the neuron star as a single object. This is just a more peculiar example of how kick can dramatically affect the evolution of a system. These results suggest that we must further investigate the details of natal kick impact on a system, considering a larger sample of binaries and taking into account directional information about $\mathbf{v}_k$ in addition to magnitude information we used here (impact of direction is introduced in sec 3.2). This could be a further development of this Thesis. Moreover, there are issues that must be solved. There is no self-consistent model of natal kicks that captures the complex physics of supernovae. We said that v_k distribution is crucial to define the merger rate of binary compact objects. Unfortunately, the number of GW events detected so far is still too low to put strong constraints on the models. Only one binary neutron star merger has been observed and the detection of a black hole-neutron star system is still missing. Finally, all the equations used in this thesis as well as the formulas included in MOBSE code suffer from several approximations. In conclusion, we can understand how important natal kicks are, especially in binary systems, but we do not have the tools to fully understand the mechanisms behind this phenomenon. For now, this remains a crucial open issue.

Bibliography

[1] B. P. Abbott, R. Abbott, T. D. Abbott, and al.

[2] R. A. Hulse and J. H. Taylor, "Discovery of a pulsar in a binary system," *Astrophys. J.*, vol. 195, pp. L51–L53, 1975.

[3] A. Einstein, "Näherungsweise Integration der Feldgleichungen der Gravitation," *Sitzungsberichte der Königlich Preußischen Akademie der Wissenschaften (Berlin*, pp. 688–696, Jan 1916.

[4] N. Giacobbo and M. Mapelli, "Revising natal kick prescriptions in population synthesis simulations," *arXiv e-prints*, p. arXiv:1909.06385, Sep 2019.

[5] P. C. Peters, "Gravitational Radiation and the Motion of Two Point Masses," *Physical Review*, vol. 136, pp. 1224–1232, Nov 1964.

[6] J. M. Weisberg and J. H. Taylor, "The Relativistic Binary Pulsar B1913+16: Thirty Years of Observations and Analysis," in *Binary Radio Pulsars* (F. A. Rasio and I. H. Stairs, eds.), vol. 328 of *Astronomical Society of the Pacific Conference Series*, p. 25, Jul 2005.

[7] B. P. Abbott, R. Abbott, and A. end al., "Observation of gravitational waves from a binary black hole merger," *Phys. Rev. Lett.*, vol. 116, p. 061102, Feb 2016.

[8] J. S. Vink, A. de Koter, and H. J. G. L. M. Lamers, "Mass-loss predictions for o and b stars as a function of metallicity," *Astron. Astrophys.*, vol. 369, pp. 574–588, 2001.

[9] J. R. Hurley, C. A. Tout, and O. R. Pols, "Evolution of binary stars and the effect of tides on binary populations," *Monthly Notices*, vol. 329, pp. 897–928, Feb 2002.

[10] P. P. Eggleton, "Aproximations to the radii of Roche lobes.," *Astrophysical Journal*, vol. 268, pp. 368–369, May 1983.

[11] G. Hobbs, D. R. Lorimer, A. G. Lyne, and M. Kramer, "A Statistical study of 233 pulsar proper motions," *Mon. Not. Roy. Astron. Soc.*, vol. 360, pp. 974–992, 2005.

[12] C. Fryer, A. Burrows, and W. Benz, "Population Syntheses for Neutron Star Systems with Intrinsic Kicks," *Astrophysical Journal*, vol. 496, pp. 333–351, Mar 1998.

[13] F. Verbunt, A. Igoshev, and E. Cator, "The observed velocity distribution of young pulsars," *Astronomy & Astrophysics*, vol. 608, p. A57, Dec 2017.

[14] P. Beniamini and T. Piran, "Formation of double neutron star systems as implied by observations," *Monthly Notices*, vol. 456, pp. 4089–4099, Mar 2016.

[15] S. Repetto, M. B. Davies, and S. Sigurdsson, "Investigating stellar-mass black hole kicks," *Monthly Notices*, vol. 425, pp. 2799–2809, Oct 2012.

[16] N. Giacobbo, M. Mapelli, and M. Spera, "Merging black hole binaries: the effects of progenitor's metallicity, mass-loss rate and eddington factor," *Monthly Notices of the Royal Astronomical Society*, vol. 474, p. 2959–2974, Nov 2017.

[17] J. R. Hurley, O. R. Pols, and C. A. Tout, "Comprehensive analytic formulae for stellar evolution as a function of mass and metallicity," *Monthly Notices*, vol. 315, pp. 543–569, Jul 2000.

[18] N. Giacobbo, M. Mapelli, and M. Spera, "Unravelling the progenitors of merging black hole binaries," in *Gravitational-waves Science Symposium*, p. 27, Mar 2018.

[19] C. L. Fryer, K. Belczynski, G. Wiktorowicz, M. Dominik, V. Kalogera, and D. E. Holz, "Compact Remnant Mass Function: Dependence on the Explosion Mechanism and Metallicity," *Astrophysical Journal*, vol. 749, p. 91, Apr 2012.